Polyoxometalate Incorporation and Effects on Proton Transport in Hydrogel Polymers

A Thesis

Presented in Partial Fulfillment of the Requirements for the

Degree of Master of Science

with a

Major in Chemical Engineering

in the

College of Graduate Studies

University of Idaho

by

Thomas Allen Christensen II

Major Professor: James G. Moberly, Ph.D.

Committee Members: Kristopher Waynant, Ph.D.; Mark Roll, Ph.D.

Department Administrator: Ching-An Peng, Ph.D.

August 2020

Authorization to Submit Thesis

This thesis of Thomas Allen Christensen II, submitted for the degree of Master of Science with a Major in Chemical Engineering and titled "Polyoxometalate Incorporation and Effects on Proton Transport in Hydrogel Polymers," has been reviewed in final form. Permission, as indicated by the signatures and dates below, is now granted to submit final copies to the College of Graduate Studies for approval.

Major Professor:	James G. Moberly, Ph.D.	Date
Committee Members:	Kristopher Waynant, Ph.D.	Date
	Mark Roll, Ph.D.	Date
Department Administrator:	Ching-An Peng, Ph.D.	Date

Abstract

Polyoxometalate clusters embedded into hydrogel biobeads may be able to solve the challenges posed by free proton generation during remediation of trichloroethylene by acting as buffers and reducing protons to hydrogen gas. In this thesis, the challenges posed by systems that contain both diffusion and reaction processes for protons are considered mathematically, and a computer simulation to was developed to prove the relationship between diaphragm cell lag period and reactive capabilities of membranes. Two polyoxometalate compounds, sodium decavanadate and alumina sulfate, were successfully incorporated into a poly(vinyl alcohol) hydrogel membrane, and the diffusivity changes associated with each compound was determined. It was found that the diffusivity of protons through an unmodified 10% w/v poly(vinyl alcohol) membrane was 1.76×10^{-5} cm^2 s^{-1}, the diffusivity through a 10%/2% w/w/v poly(vinyl alcohol)/sodium decavanadate membrane was 3.10×10^{-6} cm^2 s^{-1}, and the diffusivity through a 10%/2% w/w/v poly(vinyl alcohol)/alumina sulfate membrane was 3.32×10^{-7} cm^2 s^{-1}. Through analysis of the diaphragm cell lag period, it was found the incorporation of sodium decavanadate did not increase the reactivity of a poly(vinyl alcohol) hydrogel, and incorporation of alumina sulfate lowered the reactivity. These results indicate that polyoxometalate integration into hydrogel membranes is feasible, but does not provide any advantage to a bioremediation scenario.

Acknowledgements

I would like to thank my advisor, Dr. James Moberly, for allowing me to come crash his lab for a year and work on my Master's.

I would like to thank my other committee members, Dr. Kris Waynant and Dr. Mark Roll for ideas and guidance along the way.

I would like to thank my fellow graduate students and researchers, Jonathan Counts and Carson Silsby for pointing out where everything is, their tips and bits of advice, and the great times we had on poker nights.

I would like to thank Dr. David MacPherson for his work on the instrumentation we used and an excellent book on process control.

I would like to thank our recently retired office assistant, Gail Bergman for helping with all the little things and her bright spirit.

I would like to especially thank Zane Garner for letting me play cowboy and keep my sanity intact as I worked on my degree.

Last, but not least, I would like to thank my undergrad researcher, Conner Wootton for basically pioneering the POM syntheses that made this thesis possible and putting up with my Chris LeDoux music in lab.

This material is based upon work supported by the National Science Foundation under Grant No. (1805358). Any opinions, findings, and conclusions or recommendations expressed in this material are those of the author(s) and do not necessarily reflect the views of the National Science Foundation.

Dedication

To Dr. Heather Rothfuss.

You are the reason I wound up in Idaho.

Table of Contents

List of Figures

CHAPTER 1

Introduction

1.1 The scope of trichloroethylene contamination

Approximately 60% of all National Priority List (superfund) sites in the U.S. are contaminated with chlorinated aliphatic hydrocarbons (CAHs), including trichloroethylene (TCE), cis-1,2-dichloroethylene (DCE) and vinyl chloride (VC) (see Figure 1.1).[1] These CAHs were believed to be harmless, and were used as industrial solvents, dry-cleaning agents, and even human and veterinary anesthetics from the onset of World War I until the early 1990's.[2] At that point, epidemiological evidence found that TCE was toxic at concentrations of parts-per-billion, and also a carcinogen positively correlated with kidney, liver, and gallbladder cancers.[3] These compounds have been subsequently banned by the U.S. Environmental Protection Agency, and are all listed on the U.S. Centers for Disease Control's Agency for Toxic Substances and Disease Registry Substance Priority List, with TCE ranking as the 16th most prioritized compound, DCE the 274th, and VC the 4th.[4]

Sites contaminated with TCE and its derivatives present a unique challenge for cleanup due to the combined volatility and density of these compounds. Thanks to these properties, chlorinated solvents are able to sink to the bottom of groundwater sources where they form a phase referred to as a Dense Non-Aqueous Phase Liquid (DNAPL).[5] The most common methods for remediating a DNAPL include pump-and-treat, erecting a barrier around the source, and bioremediation.[5, 6] Of these methods, bioremediation is highly desirable thanks to its lower cost and invasiveness.

To facilitate bioremediation, soil microbes have been shown to be able to degrade chlorinated solvents naturally, and specialized consortia have even been developed that are optimized for chlorinated solvent degradation.[7, 8] Bioremediation may be an appealing strategy for decontamination, however it is not without its difficulties. One major problem is the lack of ability for microbes to facilitate bioremediation metabolism when exposed to high concentrations of chlorinated solvents, and their byproducts.[9, 10]

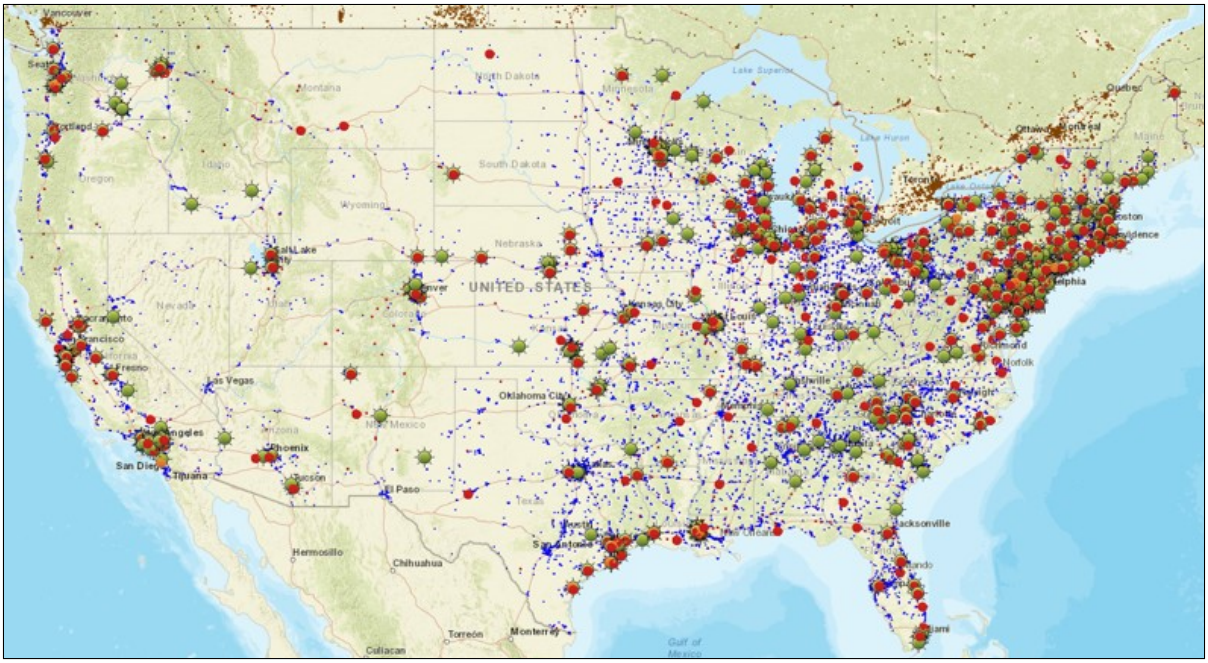

FIGURE 1.1: Chlorinated solvent-contaminated sites are present in nearly every state. Green dots represent TCE contamination, orange dots DCE, and red dots VC. Image courtesy of toxmap.nlm.nih.gov, obtained October, 2018

A simplified metabolic pathway for microbial TCE degradation is given in Figure 1.2. The pathway for degradation of TCE is based on anaerobic respiration, where the chlorinated solvent molecule serves as the electron acceptor.[11] Hydrogen, methanol, and butyrate have all been demonstrated to function as electron donors for the TCE degradation process, with hydrogen being the most energetically favorable.[12] During the degradation process, one proton from the donor molecule is substituted for a chlorine on the solvent molecule, and the freed proton and chlorine form hydrochloric acid. High concentrations of acid therefore accumulate as degradation occurs. As the species of microbes that are able to facilitate bioremediation are also highly sensitive to acidic environments, this acid generation has been shown to arrest degradation at an intermediate stage that is more toxic than the pre-remediation conditions, even in highly alkaline soil.[10]

1.2 BIOBEADS AS A SOLUTION

A proposed method for shielding microbes from toxic concentrations of TCE and protons during bioremediation is to encapsulate the microbes within a hydrogel. The gel and its encapsu-

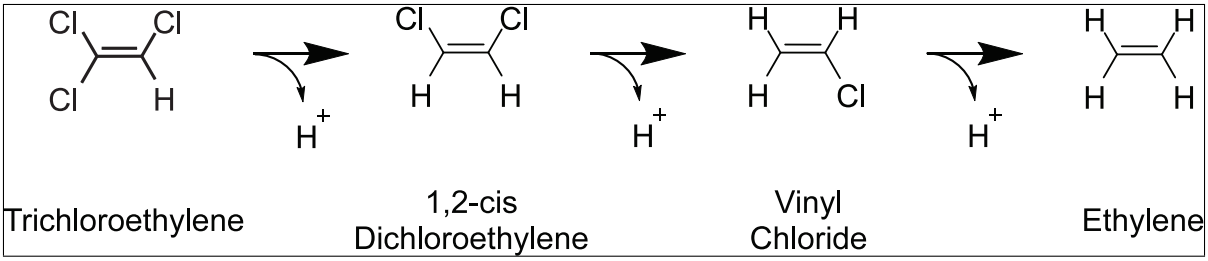

FIGURE 1.2: The process by which trichloroethylene is fully degraded results in the generation of mos toxic compounds as well as acid before finally resolving to harmless ethylene

lated microbes have been termed a "biobead."[8] Hydrogels, the main structural component of biobeads, are interlinked polymer systems where water makes up more than 20% of the total weight, and are similar in overall structure to the extracellular matrix in vertebrates or a biofilm for microbes.[13] Thanks to these properties, hydrogels are already commonly used in biological systems, such as for drug delivery, and tissue engineering.[14, 15]

Similar to how biofilms protect populations of microbes, biobeads have two main strategies for mitigating the toxic effects of an acidic environments: slowing diffusion of toxic compounds to the microbes,[16] and embedding of reactive compounds that can neutralize the toxic compounds.[17] In the case of TCE degradation, the diffusion of TCE to the microbes should be slowed to the point where it is no longer at toxic concentrations, and that the rate at which protons may diffuse away from the microbes is greater than the rate at which they are generated. In terms of reaction, little may be done to neutralize TCE coming into the bead (that is the point of bioremediation, after all), however compounds may be embedded into biobeads that can neutralize the generated acid.

1.3 POLYOXOMETALATES AS PROTON MITIGATORS

Since compounds added to a biobead will not be regenerated by the microbes it encapsulates, it is behooveful to use heterogeneous catalytic compounds within the biobead that will not be degraded upon reaction. Polyoxometalates (POMs) are compounds that meet this requirement for protons as many have been demonstrated to have reducing catalytic abilities.[18, 19]

POMs are polyatomic ions formed from oxygen complexed with metals.[20] They have been shown to have excellent ability as a reductive catalyst using the energy present in sunlight. Examples of photocatalytic reduction reactions that have been facilitated by POMs include hydrogen

generation from water[21] and alcohols[22] by polytungstates. Due to their polyionic nature and multiple protonation sites, POMs also act as excellent buffers.[23] Thanks to these two phenomena, polyoxometalates may well be suited to mitigate acid generation within a biobead, but no study has been given to this usage for POMs. Therefore, it is the purpose of this thesis to incorporate polyoxometalates into hydrogel membranes and assess their effects on proton diffusion and reaction within the hydrogel.

1.4 CONCLUSION

Trichloroethylene and the acid generated from its degradation present a challenge for remediation. Biobeads appear to be an excellent option for overcoming those challenges, and polyoxometalates may provide a method of removing generated acids from the environment. More information is needed on the methods needed to incorporate of POMs into biobeads, and testing is required to find the effects on the diffusion of protons within POM-enhanced hydrogels and the reactivity of the POMs with protons once in the hydrogel. It is the purpose of this thesis to add polyoxometalate compounds into hydrogel membranes, and examine the diffusivity and reaction capabilities of protons in these POM-enhanced hydrogels.

CHAPTER 2

The Mathematics of Reaction in a Diaphragm Cell

2.1 INTRODUCTION

In order to properly gauge the reactivity of polyoxometalates within a hydrogel, experiments must be able to distinguish between the diffusive effects and reactive effects on proton concentration within the membrane system. While methods exist for separating these effects when considering traditional solid catalyst pellets, these methods are difficult if not impossible to use on hydrogels thanks to the role that water plays in the overall structure. Therefore, in this chapter, a method of measuring reactivity using a diaphragm cell is developed, and a computer simulation was created to attempt to prove the relationship between reactivity and diaphragm cell lag period.

2.2 DIFFUSION

2.2.1 *Fick's Laws*

The mass transfer process of diffusion is typically described by Fick's First and Second Laws, given here as Equations 2.1 and 2.2 for plane wall geometry.

$$J = -\mathscr{D}\frac{\partial C}{\partial t} \tag{2.1}$$

$$\frac{\partial C}{\partial t} = \mathscr{D}\frac{\partial^2 C}{\partial x^2} \tag{2.2}$$

Where J is the flux of solute through, $\mathscr{D}$ is the diffusivity, C is the concentration of solute, t represents time, and x represents the spatial coordinate.

Diffusion in a membrane system can take place via a number of mechanisms, particularly for ionic species. For example, protons may diffuse through a membrane within the pore spaces, along the pore walls, or via isomerization reactions.[24, 25, 26] Fick's Laws are agnostic of the diffusion mechanism, however, and they may be applied with equal validity to one mechanism

at a time, or all of them acting simultaneously. For the purposes of this thesis, Fick's laws shall be applied to whole membrane systems without regard to diffusive mechanism unless otherwise noted.

The governing constant in diffusion is therefore the diffusivity. In some cases, diffusivity is not constant, but is actually a function of concentration.[27, 28] A cause for, and the implications of a concentration-dependent diffusivity will be considered in Section 2.3.2, but for most cases treating diffusivity as a constant is valid. Whether constant or concentration-dependent, diffusivity cannot be directly measured, and therefore the solution to one or both of Equations 2.1 and 2.2 must be found so available diffusion data in a model system can be used to determine diffusivity and predict real-world performance of a diffusion-reliant process. Entire volumes have been dedicated to solutions of these equations under various conditions and geometries.[27]

2.2.2 *The Diaphragm Cell*

A device called the diaphragm cell takes advantage of both simple geometry and simple boundary and initial conditions to measure diffusivity in membrane systems. The diaphragm cell was originally developed by Northop and Anson in 1929, and has since undergone several procedural and mathematical modifications to further simplify its implementation.[29, 30, 31, 32] In a diaphragm cell, a large chamber filled with high concentration of diffusing solute (the source) is separated from a chamber of little to no concentration (the sink) by a thin membrane. The concentration of solute in the sink is then measured continuously as molecules diffuse across the membrane. Westrin et al. found that the diaphragm cell is one of the most accurate devices available to measure diffusivity. When comparing the errors given by various methods of measuring diffusion, they stated "The pseudo-steady-state diaphragm cell was successful in this comparison, both with regard to accuracy and precision. The physical process in this method is slow and thus easy to monitor, and the evaluation of experimental data is straightforward."[33]

The mathematical formula for obtaining diffusivity from diaphragm cell measurements is very simple. The arrangement of the apparatus yields simple boundary conditions for the concentration profile within the membrane, namely:

1. Left boundary is always at source concentration
2. Right boundary can be found by mass balance
3. All points within membrane are at the same low concentration at the initial time point

These boundary conditions are visualized in Figures 2.1 and 2.2.

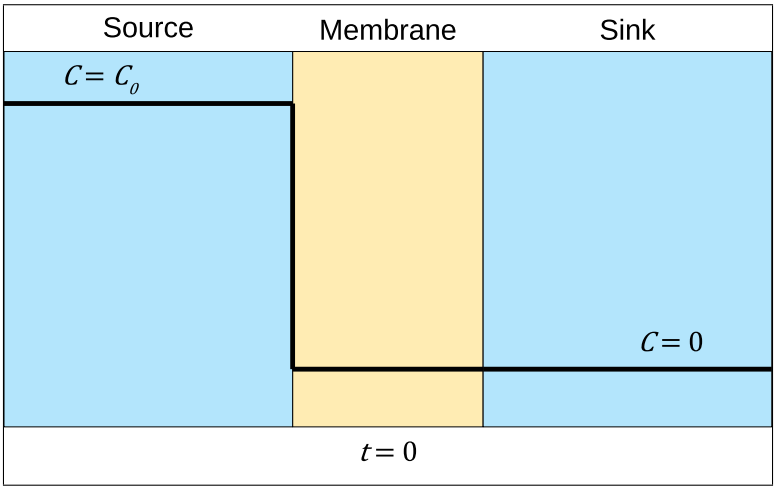

FIGURE 2.1: The initial condition of the diaphragm cell specifies that low solute concentration is present in the membrane at all points

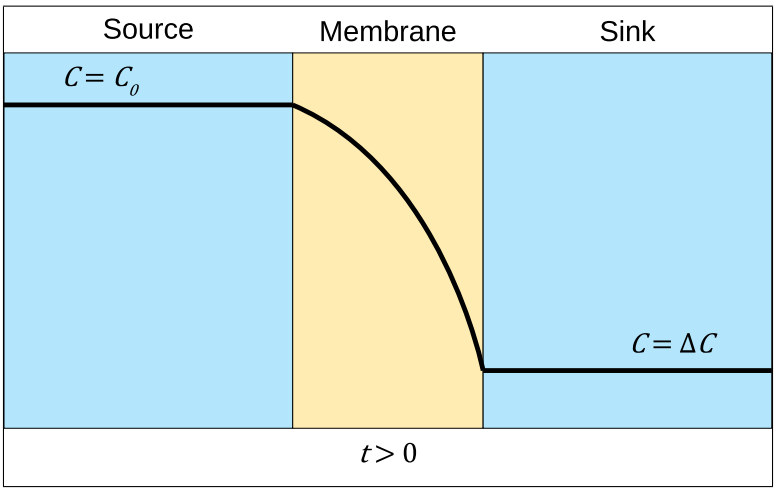

FIGURE 2.2: The boundary conditions of the diaphragm cell specify that the concentration in the source is a constant high value and the concentration in the sink is given based upon the amount of solute that has diffused through

Based on these simplifications, the slope of the concentration over time can be calculated and the diffusivity can be found using Equation 2.3.

$$\mathscr{D} = \frac{mLV}{A_c C_0} \tag{2.3}$$

Where $\mathscr{D}$ is the measured diffusivity, m is the slope of the line plotted, L is the width of the membrane, A_c is the cross-sectional area of the membrane, and C_0 is the proton concentration in the source chamber. A full derivation of Equation 2.3 is provided in Appendix A.

Naturally, there is a period of time during which no solute molecules have crossed the membrane, and therefore the sink concentration remains zero. This is referred to as the lag period, and for systems with constant diffusivity can be calculated using Equation 2.4.[24]

$$\bar{t} = \frac{L^2}{6\mathscr{D}} \tag{2.4}$$

2.2.3 *Reaction in a Diaphragm Cell*

Despite the diaphragm cell's accuracy and simplicity, neither Equation 2.3 nor Equation 2.4 take into account any reaction that may be occurring within the membrane. Other measurement methods do exist for attempting to separate the effects of diffusion and adsorption. They are based on less accurate and precise methods of determining diffusivity, however and also present their own challenges. The uptake or release of a solute from a spherical bead was one of the earliest attempts at measuring both adsorption and diffusion; the analytical solution of Fick's Laws to this system was found by Crank,[27] and has been subsequently approximated and expanded upon by others.[34] This method is extremely error-prone as the diffusivity and adsorption parameters are calculated from a single data point after the system has reached equilibrium.

Other methods allow a long membrane to come into contact with a high-concentration source and measure the concentration profile within the membrane after a set period of time has elapsed.[35, 36, 37] This method takes advantage of the simple boundary conditions applicable to a semi-infinite slab. While colored compounds may be monitored continuously to track the concentration profile,[38] transparent compounds often require experiments to be repeated and allowed to diffuse for different amounts of time before removing the membrane and cutting cross-sections to determine concentration profile. Thanks to the number of experiments, this method is costly and labor-intensive, and also retains the accuracy problems of the uptake/release method.

Given the advantages of the diaphragm cell, it would be desirable to obtain adsorption and reactivity information from diaphragm cell experiments. While not originally designed with

adsorption in mind, diaphragm cells do, however provide some information on the reactivity of solute during the diffusion process within the lag period. Although the theoretical lag period is clearly given by Equation 2.4, some systems exist which have a lag period significantly different from that predicted by Equation 2.4. An example of such a system is given in Figure 2.3.

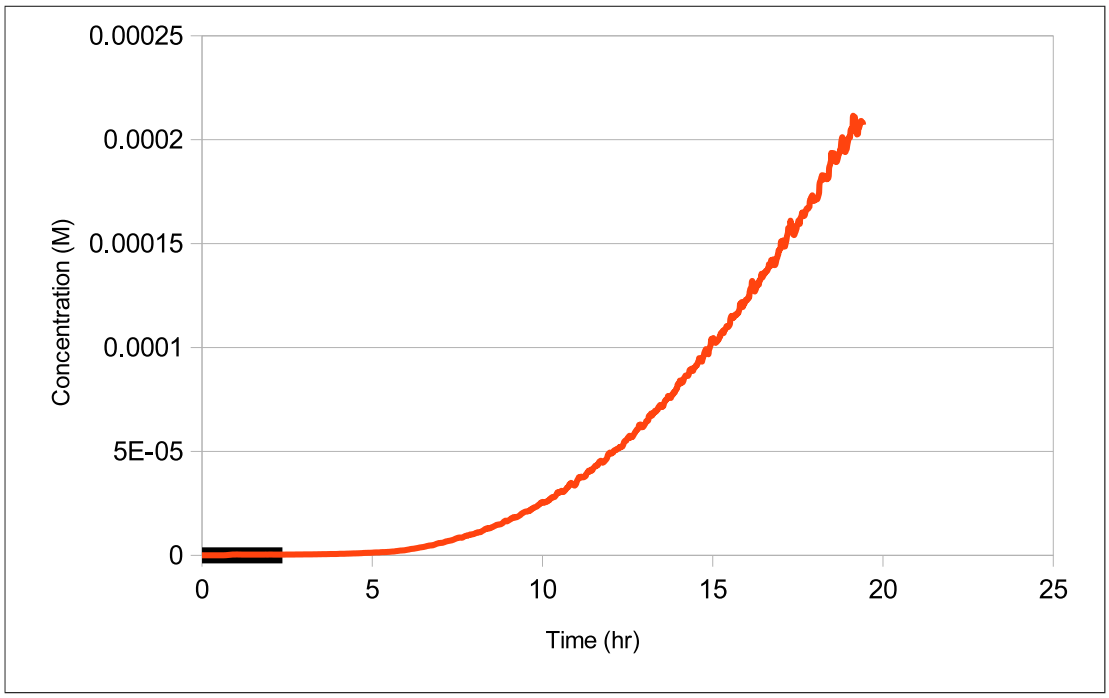

FIGURE 2.3: Diaphragm cell sink concentration time series for protons through 10% poly(vinyl alcohol). The black bar represents the expected lag period. The actual profile demonstrates that no solute enters the sink until nearly twice the lag period has elapsed.

What follows is a derivation for how reaction may be considered within a diaphragm cell, and a demonstration that such reaction may produce the type of extended lag period demonstrated in Figure 2.3

2.3 ADSORPTION

2.3.1 *Definition of Adsorption Isotherm*

The reaction of solute within a membrane in a diaphragm cell is assumed to be a heterogeneous reaction between the aqueous solute particle and the solid membrane pore surfaces. In such a case, the kinetics of binding to and release from the pore surfaces needs to be considered. When observing the outside of the membrane, as would occur for a diaphragm cell experiment,

it is difficult if not impossible to analyze these processes. Adsorption isotherms, however give relationships to find the amount of solute removed as a function of bulk concentration and kinetic rate information. A common adsorption isotherm is the Langmuir isotherm, given as Equation 2.5 which was derived from first principles based on the assumptions of a single layer of adsorbed particles and first-order reaction kinetics.[39, 40]

$$S = \frac{q_0 C}{k + C} \tag{2.5}$$

Where S is the fraction of sorbed particles, q_0 is the number of binding sites, and k is a kinetic binding reaction term.

While the fundamental nature of the Langmuir isotherm makes it desirable from a first-principles standpoint, the rational form of the equation makes it difficult to use within differential equations. A simpler expression is the Freundlich isotherm, which is an empirical relationship given by Equation 2.6.

$$S = kC^n \tag{2.6}$$

Where k and n are arbitrary constants.

2.3.2 *Adsorption in Fick's Laws*

In the cases where adsorption occurs, a modified version of Fick's Second Law applies, as shown in Equation 2.7.

$$\frac{\partial C}{\partial t} = \mathscr{D}\frac{\partial^2 C}{\partial x^2} - \frac{\partial S}{\partial t} \tag{2.7}$$

S can be found using an isotherm equation such as Equation 2.5 or Equation 2.6. The derivative can then be found and substituted directly into Equation 2.7. For example, the form of S from the Freundlich isotherm would be Equation 2.6, and its derivative would be Equation 2.8.

$$\frac{\partial S}{\partial t} = knC^{n-1}\frac{\partial C}{\partial t} \tag{2.8}$$

Substituting Equation 2.8 into Equation 2.7 yields a homogenous differential equation again, and rearranging leads to a form where all parameters are lumped together as a coefficient of the second partial term, as shown in Equation 2.9.

$$\frac{\partial C}{\partial t} = \frac{\mathscr{D}}{knC^{n-1}+1}\frac{\partial^2 C}{\partial x^2} \tag{2.9}$$

For abstraction's sake, it is convenient to define the coefficient of the second partial as an effective diffusivity $\mathscr{D}_e$, which is a function of concentration. This effective diffusivity is therefore a concentration-dependent diffusivity. Note that the term effective diffusivity has multiple meanings throughout the literature, but for the purposes of this thesis, effective diffusivity refers only to this concentration-dependent term caused by reaction within a membrane. The intrinsic diffusivity $\mathscr{D}$ describes the diffusion rate across an entire membrane regardless of mechanism, and it will be shown that $\mathscr{D}_e$ approaches $\mathscr{D}$ within a diaphragm cell as the membrane material becomes saturated with sorbed species.

2.4 METHODS

As described above, choosing an adsorption isotherm allows for the development of a concentration-dependent diffusivity $\mathscr{D}_e(C)$. As this parameter is still only in terms of the dependent variable, Equation 2.9 is a homogeneous ODE and can be numerically solved using the Crank-Nicolson method.[27] The Crank-Nicolson method is an implicit finite-difference method centered about the half-way point between steps, making it 2^{nd}-order accurate. It is stable for all step sizes, and is computationally efficient due to its use of tridiagonal matrix equations to formulate the implicit relationships. Thanks to these characteristics, the Crank-Nicolson method is well-suited to diffusion and/or adsorption problems, and when compared to analytical solutions of Fick's Law, it has been found to have "excellent agreement."[41] The Crank-Nicolson discretization of Equation 2.7 at any point i in space and any point j in time can be written as Equation 2.10.

$$\begin{aligned} -\mathscr{D}_e\left(C_{i,j}\right)\frac{\Delta t}{\Delta x^2}C_{i-1,j+1} + 2\left(1+\mathscr{D}_e\left(C_{i,j}\right)\frac{\Delta t}{\Delta x^2}\right)C_{i,j+1} - \mathscr{D}_e\left(C_{i,j}\right)\frac{\Delta t}{\Delta x^2}C_{i+1,j+1} \\ = \mathscr{D}_e\left(C_{i,j}\right)\frac{\Delta t}{\Delta x^2}C_{i-1,j} + 2\left(1-\mathscr{D}_e\left(C_{i,j}\right)\frac{\Delta t}{\Delta x^2}\right)C_{i,j} + \mathscr{D}_e\left(C_{i,j}\right)\frac{\Delta t}{\Delta x^2}C_{i+1,j} \end{aligned} \tag{2.10}$$

Where Δt is the time step size, and Δx is the spatial step size.

As there are a number of repeating terms in Equation 2.10, we introduce three new functions as Equations 2.11 through 2.13. These functions and their names have no physical or other significance: they are entirely placeholders for convenience's sake.

$$\beta\left(\eta\right) = \mathscr{D}_e\left(\eta\right)\frac{\Delta t}{\Delta x^2} \tag{2.11}$$

$$\lambda\left(\eta\right) = 2\left(1+\beta\left(\eta\right)\right) \tag{2.12}$$

$$\varepsilon\left(\eta\right) = 2\left(1-\beta\left(\eta\right)\right) \tag{2.13}$$

Substituting these new parameters into Equation 2.10, we can rewrite it as Equation 2.14.

$$\begin{aligned} -\beta\left(C_{i,j}\right)C_{i-1,j+1} + \lambda\left(c_{i,j}\right)C_{i,j+1} - \beta\left(C_{i,j}\right)C_{i+1,j+1} \\ = \beta\left(C_{i,j}\right)C_{i-1,j} + \varepsilon\left(C_{i,j}\right)C_{i,j} + \beta\left(C_{i+1,j}\right) \end{aligned} \tag{2.14}$$

A concrete example is instructive. At the time point $j = 2$ for $n = 5$ number of spatial points, Equation 2.14 becomes, in matrix form, Equation 2.15, and is visualized in Figure 2.4.

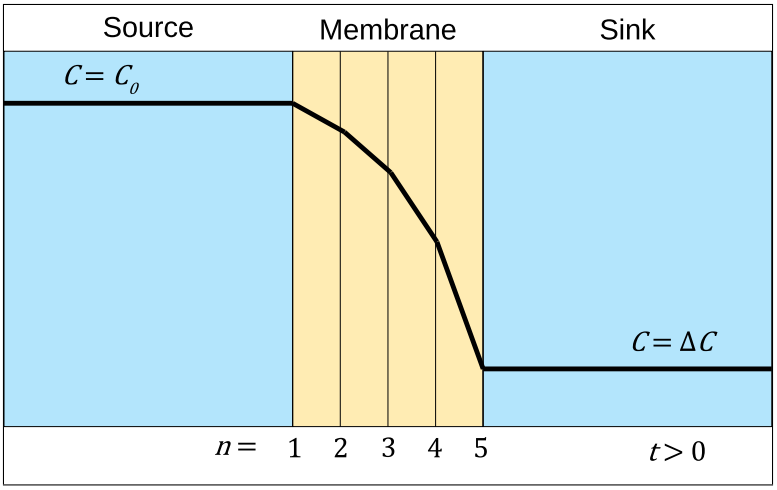

FIGURE 2.4: The discretization points for the Crank-Nicolson finite difference method as applied to a diaphragm cell membrane

$$\begin{bmatrix} \lambda(C_{1,2}) & -\beta(C_{1,2}) & 0 & 0 & 0 \\ -\beta(C_{2,2}) & \lambda(C_{2,2}) & -\beta(C_{2,2}) & 0 & 0 \\ 0 & -\beta(C_{3,2}) & \lambda(C_{3,2}) & -\beta(C_{3,2}) & 0 \\ 0 & 0 & -\beta(C_{4,2}) & \lambda(C_{4,2}) & -\beta(C_{4,2}) \\ 0 & 0 & 0 & -\beta(C_{5,2}) & \lambda(C_{5,2}) \end{bmatrix} \begin{bmatrix} C_{1,3} \\ C_{2,3} \\ C_{3,3} \\ C_{4,3} \\ C_{5,3} \end{bmatrix} = \begin{bmatrix} \varepsilon(C_{1,2}) & \beta(C_{1,2}) & 0 & 0 & 0 \\ \beta(C_{2,2}) & \varepsilon(C_{2,2}) & \beta(C_{2,2}) & 0 & 0 \\ 0 & \beta(C_{3,2}) & \varepsilon(C_{3,2}) & \beta(C_{3,2}) & 0 \\ 0 & 0 & \beta(C_{4,2}) & \varepsilon(C_{4,2}) & \beta(C_{4,2}) \\ 0 & 0 & 0 & \beta(C_{5,2}) & \varepsilon(C_{5,2}) \end{bmatrix} \begin{bmatrix} C_{1,2} \\ C_{2,2} \\ C_{3,2} \\ C_{4,2} \\ C_{5,2} \end{bmatrix} \tag{2.15}$$

Knowledge of the workings of a diaphragm cell allows us to impose boundary conditions to Equation 2.15. At the left boundary ($i = 1$), the concentration is assumed constant ($C = C_{src}$), whereas at the right boundary ($i = n$), the concentration alters based upon the flux into the sink and the sink volume, and can be found via mass balance. Although it undermines the original tridiagonal nature of Crank-Nicolson, it is convenient to place these boundary conditions directly into Equation 2.15, which gives Equation 2.16. Modern computational tools

(i.e. MATLAB) are still able to optimize the solutions to Equation 2.16 for each time step providing the necessary speed, and the stability of the Crank-Nicolson method is still valid.

$$\begin{bmatrix} 1 & 0 & 0 & 0 & 0 \\ -\beta(C_{2,2}) & \lambda(C_{2,2}) & -\beta(C_{2,2}) & 0 & 0 \\ 0 & -\beta(C_{3,2}) & \lambda(C_{3,2}) & -\beta(C_{3,2}) & 0 \\ 0 & 0 & -\beta(C_{4,2}) & \lambda(C_{4,2}) & -\beta(C_{4,2}) \\ 0 & 0 & 0 & 0 & 1 \end{bmatrix} \begin{bmatrix} C_{1,3} \\ C_{2,3} \\ C_{3,3} \\ C_{4,3} \\ C_{5,3} \end{bmatrix} \tag{2.16}$$
$$= \begin{bmatrix} 1 & 0 & 0 & 0 & 0 \\ \beta(C_{2,2}) & \varepsilon(C_{2,2}) & \beta(C_{2,2}) & 0 & 0 \\ 0 & \beta(C_{3,2}) & \varepsilon(C_{3,2}) & \beta(C_{3,2}) & 0 \\ 0 & 0 & \beta(C_{4,2}) & \varepsilon(C_{4,2}) & \beta(C_{4,2}) \\ 0 & 0 & 0 & 0 & 1 \end{bmatrix} \begin{bmatrix} C_{src} \\ C_{2,2} \\ C_{3,2} \\ C_{4,2} \\ \beta\left(C_{5,2}\right) \Delta x A_c \frac{C_{4,2}-C_{5,2}}{V} + C_{5,2} \end{bmatrix}$$

With knowledge of the concentration profile at the previous and current time steps ($j = 1, 2$), the concentration profile at the next time step ($j = 3$) can easily be solved for using Equation 2.16. Using an equation similar to Equation 2.16, a simulation was written in the MATLAB programming language to test the effects of the Freundlich isotherm on sink concentrations in a diaphragm cell. The program simulated ten spatial points within a membrane, and used approximate proton diffusivity and membrane dimensions from previous diaphragm cell experiments. Three values of k and n were tested to determine their effects on diaphragm cell output. The full source code of the program is available as Appendix B.

2.5 RESULTS

Initial drafts of the program showed that the Crank-Nicolson diaphragm cell simulation was able to mimic the extended lag period of a diaphragm cell with adsorption as seen in Figure 2.5

When varying both parameters, the length of the lag period and and curvature as the system approached steady diffusion were both affected, as shown in Figure 2.6.

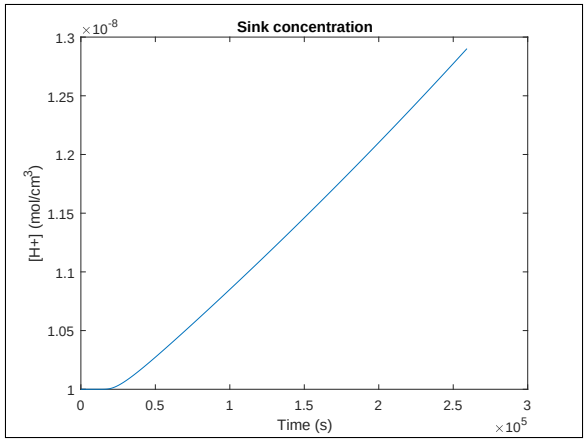

FIGURE 2.5: This simulated time series output conveys the correct shape and lag period for a diaphragm cell with Freundlich adsorption, k = 1e-3, n = 0.1

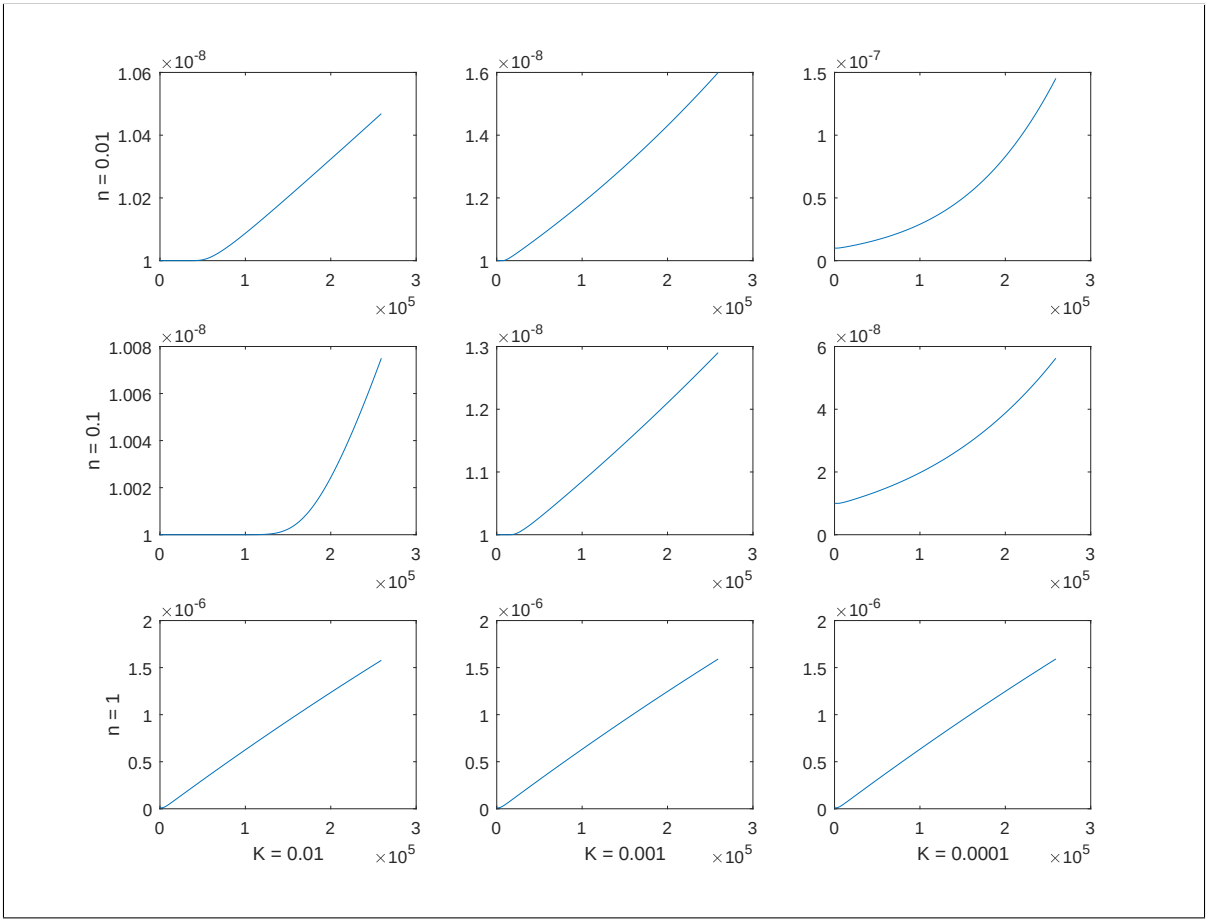

FIGURE 2.6: These simulated time series all have the same diffusivity, but differing Freundlich parameters

For a constant *n* value, it can easily be visualized on Figure 2.6 that the lag period increases as *k* increases. This is consistant with idea that *k* is an empirical affinity term, and as the affinity increases, more protons would remain sorbed within the membrane.

Also notable is how the slope of each linear section regardless of the values of n or k are identical. This is consistant with the understanding of how reaction or adsorption would work: at low concentrations within the membrane, protons are totally removed from diffusion by reaction, but as diffusion increases, the reaction reaches a steady-state. From a strictly adsorption perspective, this would mean that the membrane material has become saturated with protons, and all protons in solution are simple free to diffuse.

One last thing to note is how all graphs for $n = 1$ are perfectly identical and have a lag period exactly corresponding to expected. This arises from the form of Equation 2.9 and specifically the C^{n-1} term. When $n = 1$, $n - 1 = 0$, and therefore this term collapses to 1, and no reaction effects may be observed. While this is a rare edge case, it nonetheless is important to emphasize that in some instances, reaction may not be visible in the lag period of a diaphragm cell.

2.6 CONCLUSION

The diaphragm cell is an excellent method for determining diffusivity for constant-diffusivity species. Reaction within the membrane, however results in a variable diffusivity, which the diaphragm cell cannot adequately describe. A computer simulation was constructed to attempt to elucidate the difference between adsorption and diffusion within a diaphragm cell, and demonstrated that lag period is a function of the Freundlich adsorption parameters.

CHAPTER 3

Polyoxometalate Clusters in Hydrogels

3.1 INTRODUCTION

With a framework in place to understand proton diffusion in hydrogel membranes and adsorption or reaction taking place within that membrane, we can now afford to analyse how addition of buffers and catalysts affect the fate of protons within a biobead. As stated in Chapter 1, polyoxometalates are appealing compounds for embedding into biobeads, and the exact nature of how to embed them into hydrogels and their effects and stability when embedded are unknown.

An ideal polyoxometalate (POM) for embedding into biobeads should have the ability to catalyze hydrogen reduction at mild conditions. For this requirement, decatungstate matches very well, as it has the ability to reduce many compounds with no more for energy requirements than sunlight.[18, 21, 42, 43] Unfortunately, previous work has demonstrated that decatungstate clusters are unstable in water, and unsuitable in that regard for inclusion in hydrogel biobeads.

A similar compound in terms of charge and structure is decavanadate.[44] This similarity is useful for overall comparisons, however it must be stressed that significant differences exist between the two compounds: the most notable being that decavanadate is stable in water and that decavanadate is unable to catalytically reduce protons to hydrogen.[45, 23] These distinctions do provide an advantage, as it allows for the study of strictly buffering effects within POM-enhanced biobeads.

While tungstates and vanadates have the ability to buffer protons thanks to their multiple anionic sites, other POMs exist that may have reactive capabilities even while possessing cationic charge. An example of a polycationic polyoxometalate is alumina. Alumina can be synthesized in the form of a sulfate salt that can be added to hydrogels.[46, 47] To investigate the role that POM charge may have on diffusion and adsorption, the diffusivity, reactivity, and any structural changes would need to be measured in both a cationic POM-enhanced hydrogel and an anionic POM-enhanced hydrogel and compared.

With this in mind, it was the goal of this chapter to create both decavanadate- and alumina-enhanced poly(vinyl alcohol) hydrogels and examine the structural, diffusive, and reactive changes caused by the inclusion of the POM.

3.2 MATERIALS AND METHODS

3.2.1 *Sodium Decavanadate Cluster Synthesis*

The synthesis of sodium decavanadate closely followed the procedure given by Johnson et al,[48] and is as follows: 5 g (0.041 mol) of sodium metavanadate (Strem Chemicals) was dissolved into 10 mL of water and heated to 30 °C. Upon reaching temperature, 0.5 mL of glacial acetic acid (Fisher Scientific) was added once every minute for 10 minutes, resulting in exactly 5 mL (0.114 mol) added total. The solution's temperature was brought down to 25 °C for 1 hour. The solution was then gravity filtered on paper and rinsed liberally with acetone.

After being allowed to dry for 1 hour, the solid product was dissolved into 10 mL of fresh water, and heated to 50 °C. Upon all product being dissolved, the solution was immediately filtered through a 1.0 μm borosilicate microfiber filter, and the filtrate was placed into a 4 °C refrigerator for 12 hours, during which time the purified product would crash out of solution. After 12 hours, the filtrate was again gravity filtered on paper, using minimal amounts of acetone for rinsing as needed. Upon fully drying the filter cake was collected as the product.

Samples were assessed for purity using a UV-Visible spectrum of 8.8×10^{-3} M decavanadate solution in water at 200-400 nm wavelength, and compared to the reference spectra given by Goddard and Gonas.[45]

3.2.2 *Alumina Sulfate Cluster Synthesis*

The procedure for synthesis of alumina sulfate was adapted from those given in Johansson,[46] and Wang and Muhammed,[47] and is as follows: 3.6215 g (0.0150 mol) of aluminum chloride 6 hydrate (Mallinckrodt Chemical) was dissolved in 150 mL MilliQ water to make a 0.1 M solution and heated to 80 °C. Upon reaching temperature, 2.5 molar equivalents of sodium hydroxide (Sigma-Aldrich) was added in the form of 37.5 mL of 1 M solution. The system was then kept at 80 °C for 30 minutes, after which at least 5.4323 g (0.0382 mol) of sodium sulfate (Baker Chemical) was added, and the solution was then covered and refrigerated at 4 °C for one week.

After one week of refrigeration, crystals had precipitated and settled to the bottom of the solution. The solution and precipitate were then gravity or vacuum filtered for upwards of 6 hours until dry and brittle. Filter cake was then ground to a fine powder using a mortar and pestle.

Purity of each synthesis was evaluated using powder x-ray diffraction.

3.2.3 *Membrane Preparation*

Four types of poly(vinyl alcohol) (PVA) (MW: 146-186 kg/mol, ACROS Organics) hydrogel membranes were cast for this study. Each membrane type was constructed such that the composition would be 10% PVA by weight and 2% other compound of interest by weight. The exception to this was the control membranes, which simply omitted the other compound, resulting in a 10% PVA by weight hydrogel. 10%/2% hydrogels were made of each POM compound (sodium decavanadate and alumina sulfate), and also a 10%/2% membrane of sodium alginate (SA) (Sigma-Aldrich), an anionic hydrogel compound, was created to help make comparisons based on membrane charge.

Membranes were created as follows: 5 g of poly(vinyl alcohol) and 1 g of the compound of interest were dissolved into 50 mL of water at 80 °C and allowed to fully homogenize. The molten membrane was then refrigerated overnight. Molten membrane was reheated to 40 °C before casting. To cast, membrane solution was poured into custom-machined porous PVC molds that could be directly embedded into the GellipHish diaphragm cell (see below). A drawing of such a mold is shown in Figure 3.1.

It should be noted that alumina sulfate clusters are not highly soluble in water, but when finely ground, they could be evenly suspended throughout the entire membrane solution. No settling of clusters during any step of their preparation or use was observed, and even distribution of alumina clusters throughout the entire membrane was observed via microscopy (see Section 3.3.3).

Membrane molds were filled at least one-quarter of the way full, then to crosslink, the membranes were successively frozen at -20 °C for 2 hours and thawed at room temperature for 2 hours for five complete cycles. Physical crosslinking via freeze/thaw cycles was chosen rather than chemical cross-linking to avoid the effects that the crosslinker might have on the POMs within the gel. Freeze/thaw crosslinking has been demonstrated to be very effective for poly(vinyl

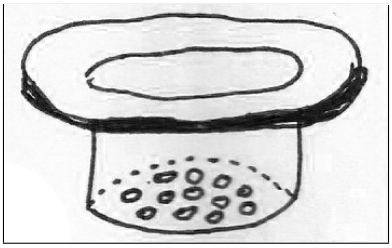

Figure 3.1: A representative membrane mold that was used

alcohol) gels,[49, 50] and no structural soundness issues were experienced in this study. Upon completion of the last cycle, membranes were immersed in water overnight before use.

3.2.4 *GellipHish Diaphragm Cell*

A custom triplicate diaphragm cell apparatus (nicknamed the GellipHish due to its appearance, instrumentation and purpose) was constructed from 1-½" diameter PVC pipe (see Figure 3.2).

3 ~100 mL capacity chambers (sinks) were inserted into a 4-way PVC junction such that 1 membrane would separate each chamber from the junction. A large (> 500 mL capacity) chamber (source) was attached to the remaining point on the junction. See Figure 3.3 for a cutaway drawing of this setup.

92 mL of deionized water and a stir bar was then added to each sink chamber and sealed with a pH probe inserted into a waterproof connector. The source chamber was then filled with aqueous hydrochloric acid (pH ~2.3) and a stir bar was added. The pH probes took continuous measurements and the pH in each chamber was recorded using a Raspberry Pi computer and a custom Python script.

3.2.5 *Thin Sectioning*

In order to qualitatively evaluate the success of incorporating both POMs into the hydrogel membranes, thin sections were taken and photographed using light field optical microscopy. Membranes were also acid-treated to simulate the effects of a diaphragm cell experiment to check for any structural differences that may have occurred while in an acidic environment.

Membranes were prepared as described in Section 3.2.3, then after soaking in deionized water, membranes of each compound were placed into either a fresh deionized water bath or an acid bath of pH ~2.3 and allowed to soak for an additional 2 days. After completion of the

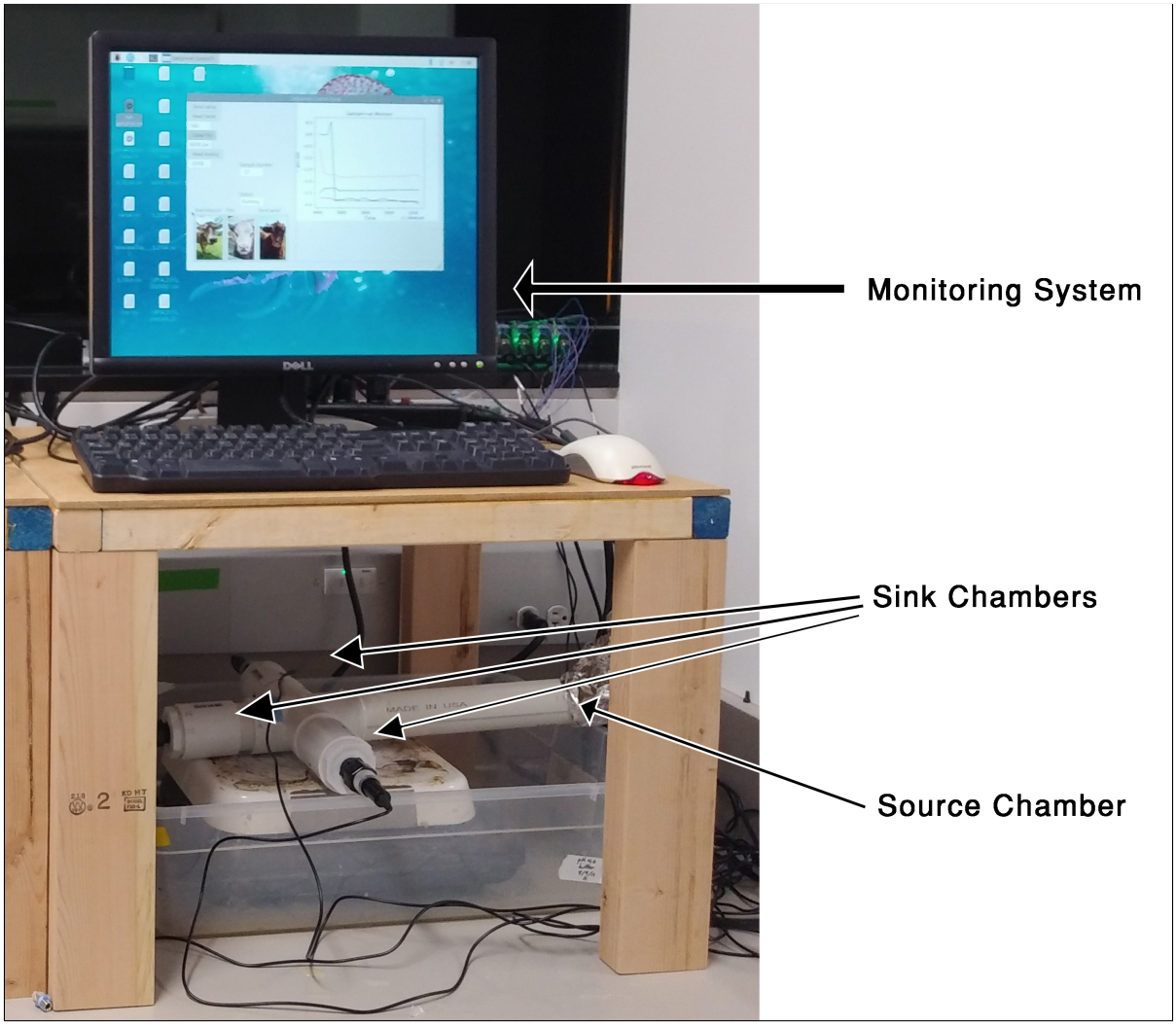

FIGURE 3.2: Photograph of the GellipHish Setup

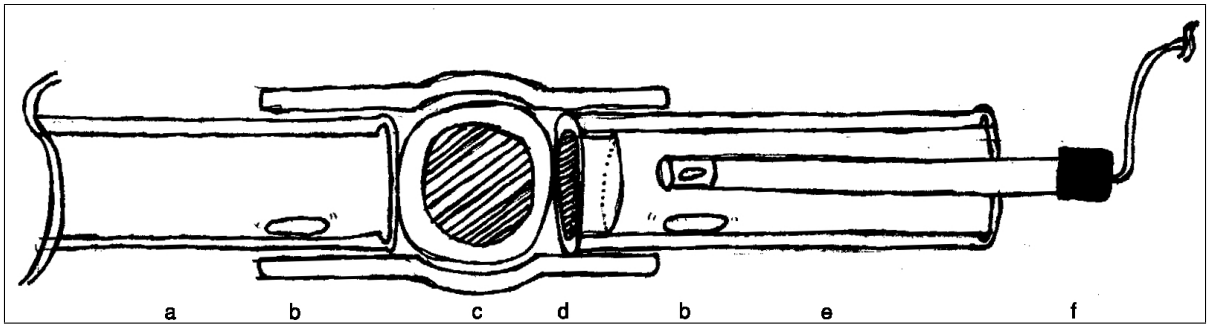

FIGURE 3.3: Cutaway drawing of the interior of the GellipHish diaphragm cell. a: source chamber, b: stir bars, c: t-junction, d: membrane and puck, e: sink chamber, f: pH probe

soaking, the membranes were removed from their baths and frozen for 2 hours at -20 °C, at which point they were then cut into rough sections. Rough sections could then be used directly

or stored for future use at -20 °C. For analysis, each rough section was placed into the sample holder of a Leica UltraCut microtome, and cooled to -80 °C for a minimum of 2 hours. The frozen sample was sliced into 15 μm thin slices using the microtome at room temperature, and immediately transferred to a glass slide and imaged.

3.3 RESULTS

3.3.1 *Diffusivity*

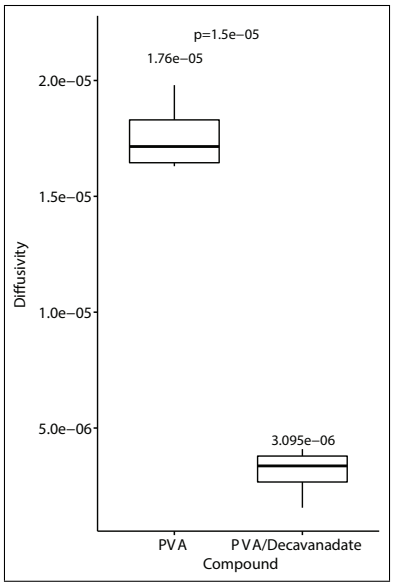

FIGURE 3.4: Proton diffusivity through 10% PVA and 10%/2% PVA/sodium decavanadate physically crosslinked hydrogel membranes

Diffusivities were calculated using the methods described in Section 2.2.2 and Equation 2.3. The diffusivity of protons in a PVA/decavanadate membrane was found to be 3.10×10^{-6} cm^2 s^{-1}, nearly an order of magnitude less than the diffusivity in the control PVA membrane 1.76×10^{-5} cm^2 s^{-1} (Welch t-test, $p = 1.74 \times 10^{-5}$) (see Figure 3.4). A useful comparison is to the similarly charged hydrogel system, PVA/sodium alginate. As shown in Figure 3.5, PVA and PVA/sodium alginate do not have significantly different diffusivities (Welch t-test, $p = 0.97$) despite the formal charge differences. It can then be concluded that the ionic nature of decavanadate alone is not responsible for the change in diffusivity.

When comparing Alumina-enhanced PVA to unmodified PVA, alumina decreased the diffusivity to 3.32×10^{-7}cm^2 s^{-1}, nearly two orders of magnitude less than the diffusivity through

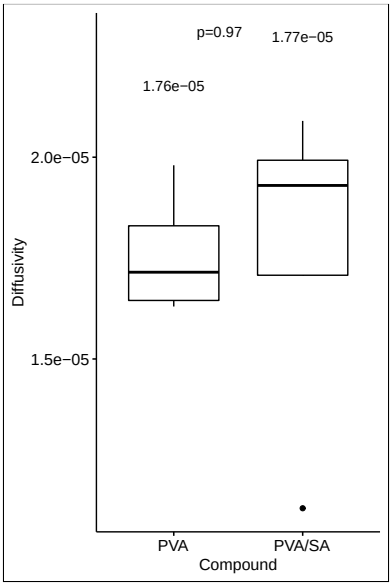

FIGURE 3.5: Proton diffusivity through 10% PVA and 10%/2% PVA/sodium alginate physically crosslinked hydrogel membranes

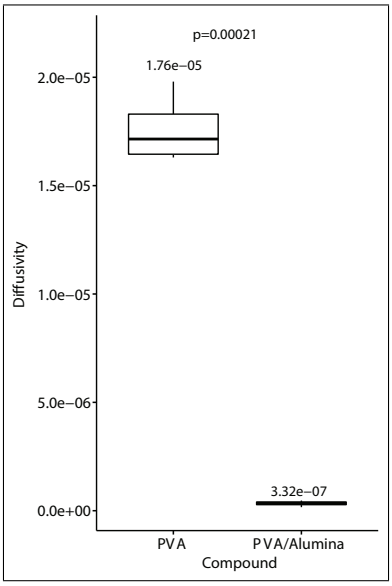

FIGURE 3.6: Proton diffusivity through 10% PVA and 10%/2% PVA/alumina sulfate physically crosslinked hydrogel membranes

standard PVA (Welch t-test, $p = 2.16 \times 10^{-4}$, see Figure 3.6). This diffusivity is also significantly lower than the diffusivity through decavanadate-enhanced PVA (Welch t-test, $p = 0.0149$, see Figure 3.7). These range of results indicate that charge alone provides no predicable effect on diffusivity, however they provide little information on the suitability of POMs into biobeads.

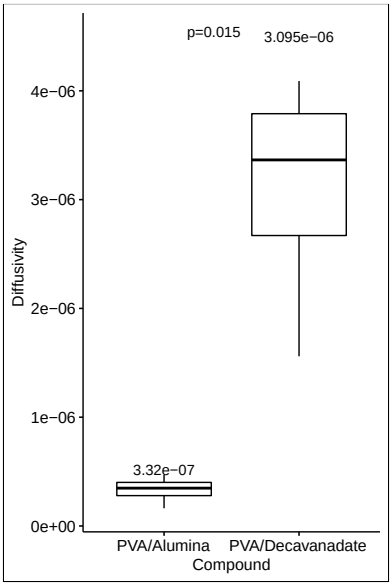

FIGURE 3.7: Proton diffusivity through 10%/2% PVA/alumina sulfate and 10%/2% PVA/sodium decavanadate physically crosslinked hydrogel membranes

What these changes in diffusivity do provide is a frame of reference from which information regarding reactivity can be properly gauged.

3.3.2 *Lag Periods*

Lag periods were found as the x-intercept of the lines used to determine the diffusivity, as described in Siepmann and Siepmann.[51]. In order to normalize for the length and diffusivity differences between membranes, lag period was compared as a fractional lag period based upon the expected lag period given by Equation 2.4. The normalized lag period is given by Equation 3.1 and referred to progammatically as "Lag_Frac."

$$\bar{t}_{frac} = \frac{\bar{t}}{\frac{L^2}{6\mathscr{D}}} \tag{3.1}$$

Where $\bar{t}$ refers to the measured lag period.

The control PVA membranes were found to have a fractional lag period of 4.95 and the decavanadate-enhanced membranes had a fractional lag period of 4.8 (see Figure 3.8). These were not significantly different (Welch t-test, $p = 0.87$). This is not entirely unexpected as decavanadate has no catalytic potential for reacting with protons within the membrane, although some buffering action might have been expected to increase the lag period. Comparing once

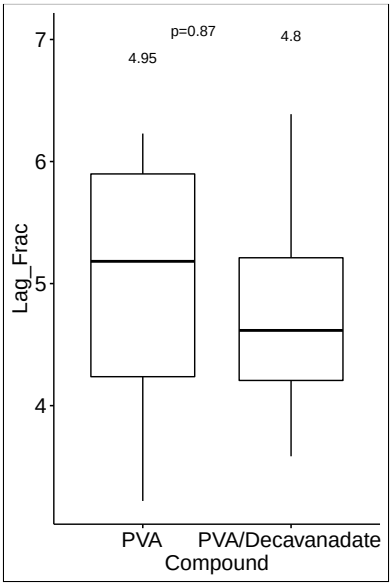

FIGURE 3.8: Fractional diaphragm cell lag periods for protons through 10% PVA and 10%/2% PVA/sodium decavanadate physically crosslinked hydrogel membranes

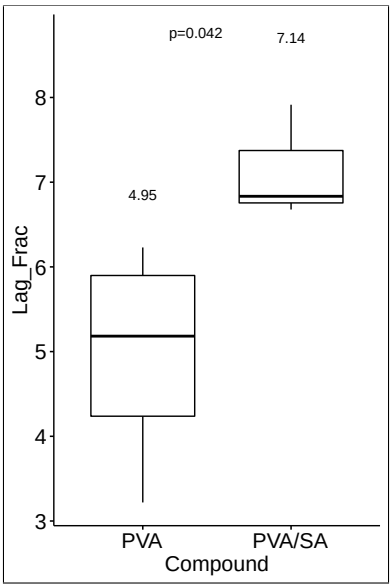

FIGURE 3.9: Fractional diaphragm cell lag periods for protons through 10% PVA and 10%/2% PVA/sodium alginate physically crosslinked hydrogel membranes

again to PVA/alginate (see Figure 3.9) as a way to examine charge effects, the inability of decavanadate to increase the lag period is surprising however, as alginate does significantly increase the fractional lag period to 7.14 (Welch t-test, $p = 0.042$).

With the potential capabilities of PVA/alumina for proton reaction, it would be expected that PVA/alumina would increase the fractional lag period. As shown in Figures 3.10 and 3.11

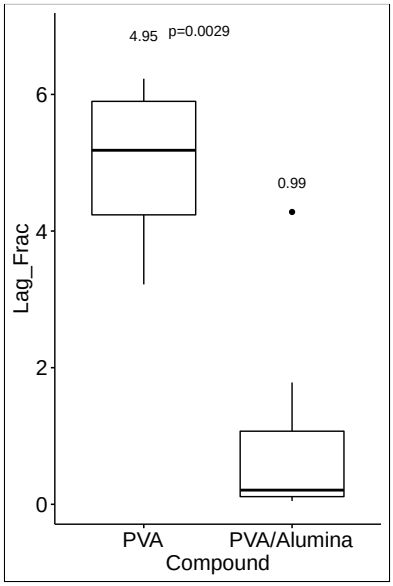

FIGURE 3.10: Fractional diaphragm cell lag periods for protons through 10% PVA and 10%/2% PVA/alumina sulfate physically crosslinked hydrogel membranes

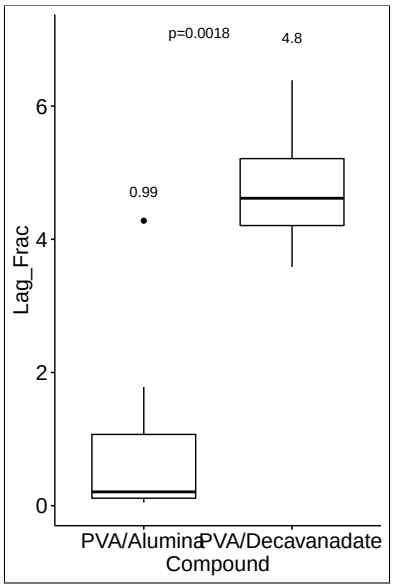

FIGURE 3.11: Fractional diaphragm cell lag periods for protons through 10%/2% PVA/alumina sulfate and 10%/2% PVA/sodium decavanadate physically crosslinked hydrogel membranes

however, this is not the case. Instead, the fractional lag period through PVA/alumina is 0.99, meaning that incorporation of alumina into PVA brings the lag period back to its expected value as given by Equation 2.4. This change is significantly different from both control PVA (Welch t-test, $p = 2.9 \times 10^{-3}$) and also PVA/decavanadate (Welch t-test, $p = 1.8 \times 10^{-3}$). Thanks to this

decrease in lag period, it may be concluded that alumina does not, in fact react with any protons diffusing through the hydrogel.

3.3.3 *Thin Sections*

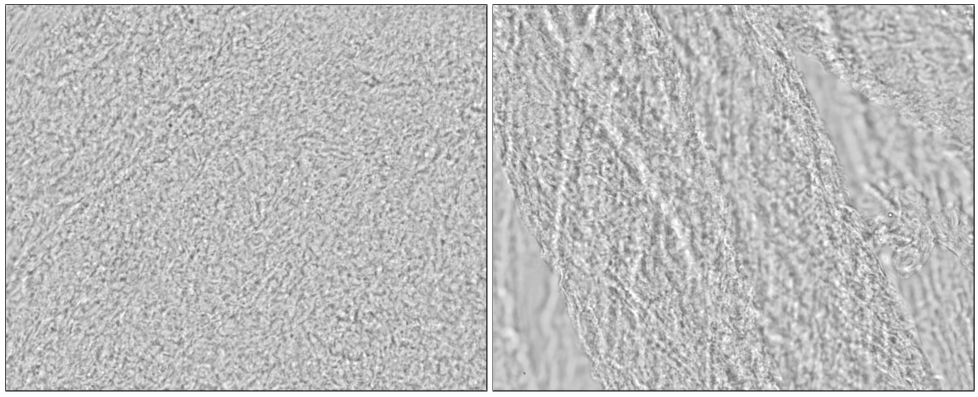

(A) Control (B) Acid-Treated

FIGURE 3.12: Microscopy images of 10% PVA 5-cycle freeze/thaw crosslinked hydrogel membranes at 20x zoom

Images of PVA show a rough but uniform surface across the entire membrane regardless of exposure to acid, as shown in Figure 3.12.

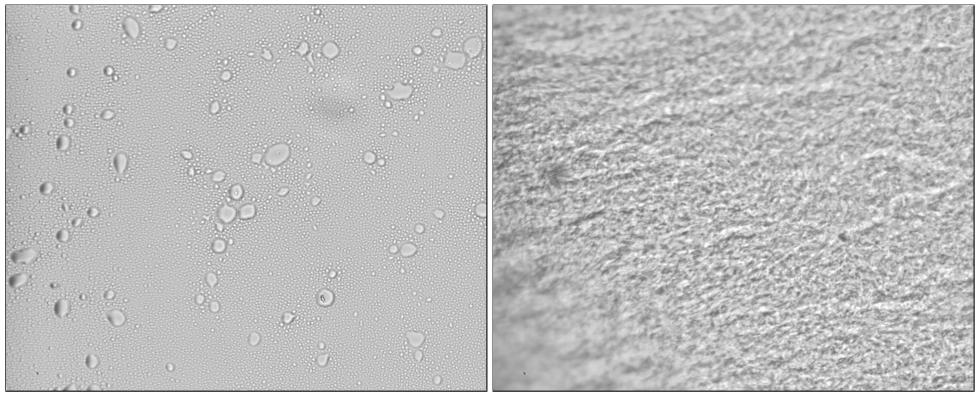

(A) Control (B) Acid-Treated

FIGURE 3.13: Microscopy images of 10%/2% PVA/sodium decavanadate 5-cycle freeze/thaw crosslinked hydrogel membranes at 20x zoom

When compared to unmodified PVA, images of decavanadate-enhanced membranes show some unique features, as shown in Figure 3.13. The most apparent is the appearance of circular structures throughout the membrane surface and the lack of roughness shown before exposure

to acid. It should be emphasized that these structures are not air pockets, though the digital images make them appear very similar to air pockets. After acid treatment, the decavanadate membranes appear very similar in structure to a control PVA membrane. It is hypothesized that these circular structures are clusters of decavanadate, and that under acidic conditions, these clusters more evenly disperse throughout the membrane. This is consistent with the knowledge that decavanadate is prepared under acidic conditions, that no reaction was observed to take place within a decavanadate-enhanced membrane, and that decavanadate membranes still have the distinctive orange color after acid treatment. Further testing would be required to demonstrate the validity of this hypothesis, however.

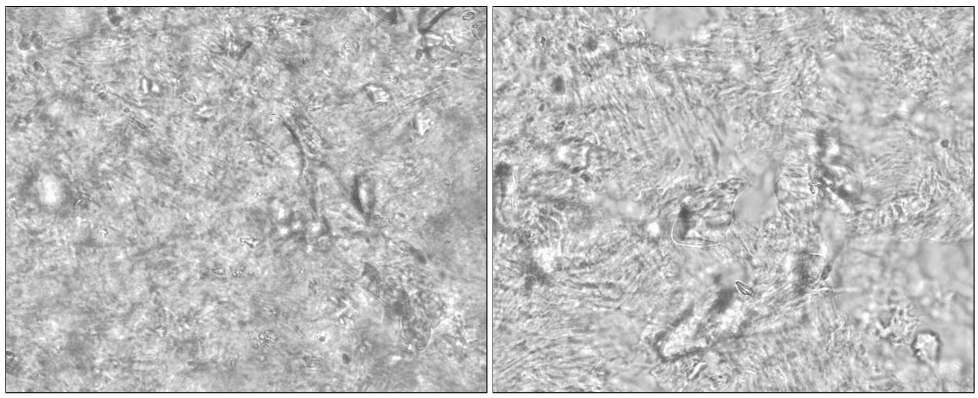

(A) Control (B) Acid-Treated

FIGURE 3.14: Microscopy images of 10%/2% PVA/alumina sulfate 5-cycle freeze/thaw crosslinked hydrogel membranes at 20x zoom

Alumina-enhanced membranes, as shown in Figure 3.14, demonstrate clear crystal portions distributed throughout the entire membrane. These crystals do not change with exposure to acid, as would be consistent with the observation of no reaction occurring in a PVA/alumina hydrogel.

3.4 CONCLUSION

Two polyoxometalate compounds, sodium decavanadate and alumina sulfate, were successfully incorporated into poly(vinyl alcohol) hydrogels, as was verified using optical microscopy. Both POMs decreased the diffusivity of protons within the hydrogel. Lag period calculations demonstrated that no proton-consuming reactions occurred in either POM-enhanced membrane, how-

ever. Microscopy images of the alumina-enhanced membranes further suggested no reaction occurring within them.

CHAPTER 4

Conclusion

4.1 CONCLUSIONS

This work examined the feasibility and implications of incorporating polyoxometalates into hydrogel biobeads. Based upon the results found here, it appears that polyoxometalate incorporation into hydrogel biobeads does not provide a suitable strategy for mitigating the problem of acid generation during TCE remediation.

First, it is noted that both POM compounds that were tested decreased the diffusivity of protons through the PVA/POM hydrogels. This is undesirable, as it would not allow for the acid conditions to dissipate into the surroundings as quickly. While this is a negative consequence of POM integration, it could be overcome by even slower TCE diffusion rates, and may actually be desirable if protons could be removed via reaction.

Additional reaction due to POM integration was not observed, however, as evidenced by no increase in lag period combined with the relationship between lag period and reactivity developed in Chapter 2. Addition of decavanadate demonstrated no additional reaction capability with protons than the control PVA membranes, and addition of alumina dramatically decreased it. In addition, the thin section microscopy of the alumina membranes demonstrated no visible changes in the membranes upon exposure to acid conditions, further indicating that alumina is unreactive with protons when incorporated into hydrogels.

In spite of the lack of reaction shown by POMs, the ability to alter the proton diffusivity over two orders of magnitude shows some promise in being able to fine-tune the diffusivity of protons through PVA membranes. If in some instance a specific diffusivity is required for biobead design, POMs might provide a strategy for manipulating the diffusivity to that value.

4.2 FUTURE WORK

In spite of the failure of the tested POMs to react with protons while incorporated into a PVA membrane, some work still needs to be done in order to fully accept or dismiss the usefulness of POMs in bioremediation.

Different concentrations of the POMs into hydrogels (*e.g.* 10%/1% PVA/decavanadate) need to be investigated to find the diffusivity dependence on POM concentration. Ideally, a relationship between POM concentration and diffusivity would allow for finely-tuned biobeads as described above.

An anionic reducing POM (*e.g.* decatungstate) also needs to be evaluated for diffusivity and reactivity changes. The comparison between decavanadate and alumina are informative, but convolute the concepts of charge and reactivity. In addition, since decatungstate specifically has been shown to facilitate hydrogen generation, evaluating it directly would be far more informative on the reactive capabilities of POMs than those tested here. While decatungstate was dismissed previously due to stability issues, some of the work presented here may allow for development of an improved handling system to overcome those difficulties.

Toxicity issues of POMs in hydrogels must also be evaluated. POMs often damage cells that are in contact for extended periods of time, but incorporation into hydrogels has been shown to decrease these effects.[52] As microbial viability is the central goal of a biobead system, the toxicity element needs to clearly addressed.

Once at least one of these elements has been further investigated, it can be stated more emphatically whether polyoxometalates truly present a worthy addition to biobeads for trichloroethylene remediation.

References

[1] US EPA O. Superfund: National Priorities List (NPL). https://www.epa.gov/superfund/superfund-national-priorities-list-npl 2015.

[2] Doherty RE. A History of the Production and Use of Carbon Tetrachloride, Tetrachloroethylene, Trichloroethylene and 1,1,1-Trichloroethane in the United States: Part 1—Historical Background; Carbon Tetrachloride and Tetrachloroethylene. *Environmental Forensics.* 2000;1:69-81.

[3] US Environmental Protection Agency National Center for Environmental Assessment . Trichloroethylene. Tech. Rep. CASRN 79-01-6 2011.

[4] Substance Priority List | ATSDR. https://www.atsdr.cdc.gov/spl/index.html 2020.

[5] Huling SG, Weaver JW. GROUND WATER ISSUE: DENSE NONAQUEOUS PHASE LIQUIDS. Tech. Rep. 540/4-91/002U.S. Environmental Protection AgencyWashington, D.C. 1991.

[6] Yang Y, McCarty PL. Biologically Enhanced Dissolution of Tetrachloroethene DNAPL. *Environmental Science & Technology.* 2000;34:2979-2984.

[7] Kim S, Bae W, Hwang J, Park J. Aerobic TCE degradation by encapsulated toluene-oxidizing bacteria, Pseudomonas putida and Bacillus spp. *Water Science and Technology.* 2010;62:1991-1997.

[8] Zhou Yz, Yang J, Wang Xl, et al. Bio-beads with immobilized anaerobic bacteria, zero-valent iron, and active carbon for the removal of trichloroethane from groundwater. *Environmental Science and Pollution Research International; Heidelberg.* 2014;21:11500-9.

[9] Haest PJ, Springael D, Smolders E. Dechlorination kinetics of TCE at toxic TCE concentrations: Assessment of different models. *Water Research.* 2010;44:331-339.

[10] Robinson C, Barry DA, McCarty PL, Gerhard JI, Kouznetsova I. pH control for enhanced reductive bioremediation of chlorinated solvent source zones. *Science of The Total Environment.* 2009;407:4560-4573.

[11] Cretnik S, Bernstein A, Shouakar-Stash O, Löffler F, Elsner M. Chlorine Isotope Effects from Isotope Ratio Mass Spectrometry Suggest Intramolecular C-Cl Bond Competition in Trichloroethene (TCE) Reductive Dehalogenation. *Molecules.* 2014;19:6450-6473.

[12] Aulenta F, Gossett JM, Papini MP, Rossetti S, Majone M. Comparative study of methanol, butyrate, and hydrogen as electron donors for long-term dechlorination of tetrachloroethene in mixed anerobic cultures. *Biotechnology and Bioengineering.* 2005;91:743-753.

[13] Cai W, Gupta RB. Hydrogels. in *Kirk-Othmer Encyclopedia of Chemical Technology*:1-20American Cancer Society 2012.

[14] Langer R. New methods of drug delivery. *Science.* 1990;249:1527-1533.

[15] Vu TTT, Lim C, Lim M. Characterization of leukemic cell behaviors in a soft marrow mimetic alginate hydrogel. *Journal of Biomedical Materials Research Part B: Applied Biomaterials.* 2012;100B:1980-1988.

[16] Stewart PS. Diffusion in Biofilms. *Journal of Bacteriology.* 2003;185:1485-1491.

[17] Takenaka S, Pitts B, Trivedi HM, Stewart PS. Diffusion of Macromolecules in Model Oral Biofilms. *Applied and Environmental Microbiology.* 2009;75:1750-1753. 00039.

[18] Texier I, Giannotti C, Malato S, Richter C, Delaire J. Solar photodegradation of pesticides in water by sodium decatungstate. *Catalysis Today.* 1999;54:297-307.

[19] Protti S, Ravelli D, Fagnoni M, Albini A. Solar light-driven photocatalyzed alkylations. Chemistry on the window ledge. *Chemical Communications.* 2009:7351-7353.

[20] Gómez-Romero P, Lira-Cantú M. Hybrid Nanocomposite Materials. in *Kirk-Othmer Encyclopedia of Chemical Technology*American Cancer Society 2002.

[21] Akid R, Darwent JR. Heteropolytungstates as catalysts for the photochemical reduction of oxygen and water. *Journal of the Chemical Society, Dalton Transactions.* 1985:395.

[22] Yamase T, Takabayashi N, Kaji M. Solution photochemistry of tetrakis(tetrabutylammonium) decatungstate(VI) and catalytic hydrogen evolution from alcohols. *Journal of the Chemical Society, Dalton Transactions.* 1984:793.

[23] Capparelli MV, Goodgame DML, Hayman PB, Skapski AC. Protonation sites in the decavanadate ion: X-ray crystal structure of tetrakisadenosinium dihydrodecavanadate(V) undecahydrate. *Journal of the Chemical Society, Chemical Communications.* 1986:776-777.

[24] Crank J. , ed.*Diffusion in Polymers.* London: Acad. Pr3. print ed. 1977. OCLC: 256041794.

[25] Amsden B. Solute Diffusion within Hydrogels. Mechanisms and Models. *Macromolecules.* 1998;31:8382-8395. 00793.

[26] Agmon N. The Grotthuss mechanism. *Chemical Physics Letters.* 1995;244:456-462.

[27] Crank J. *The Mathematics of Diffusion.* Oxford: Oxford, Clarendon Press 1956.

[28] Ruthven DM. Sorption kinetics for diffusion-controlled systems with a strongly concentration-dependent diffusivity. *Chemical Engineering Science.* 2004;59:4531-4545.

[29] Northrop JH, Anson ML. A Method for the Determination of Diffusion Constants and the Calculation of the Radius and Weight of the Hemoglobin Molecule. *The Journal of General Physiology.* 1929;12:543-554.

[30] Gordon AR. The Diaphragm Cell Method of Measuring Diffusion. *Annals of the New York Academy of Sciences.* 1945;46:285-308.

[31] Stokes RH. An Improved Diaphragm-cell for Diffusion Studies, and Some Tests of the Method. *Journal of the American Chemical Society.* 1950;72:763-767. 00329.

[32] Dullien FaL, Shemilt LW. Equations for determining Diffusion Coefficients in Liquid Systems by the Diaphragm Cell Technique. *Nature.* 1960;187:767-768.

[33] Westrin BA, Axelsson A, Zacchi G. Diffusion measurement in gels. *Journal of Controlled Release.* 1994;30:189-199.

[34] Vermeulen T. Theory for Irreversible and Constant-Pattern Solid Diffusion. *Industrial & Engineering Chemistry.* 1953;45:1664-1670.

[35] Mavituna F, Park JM, Gardner D. Determination of the effective diffusion coefficient of glucose in callus tissue. *The Chemical Engineering Journal.* 1987;34:B1-B5. 00019.

[36] Johansson L, Löfroth JE. Diffusion and interaction in gels and solutions: I. Method. *Journal of Colloid and Interface Science.* 1991;142:116-120. 00043.

[37] Xu T, Fu R. Determination of effective diffusion coefficient and interfacial mass transfer coefficient of bovine serum albumin (BSA) adsorption into porous polyethylene membrane by microscope FTIR-mapping study. *Chemical Engineering Science.* 2004;59:4569-4574.

[38] Perullini M, Jobbágy M, Japas ML, Bilmes SA. New method for the simultaneous determination of diffusion and adsorption of dyes in silica hydrogels. *Journal of Colloid and Interface Science.* 2014;425:91-95.

[39] Langmuir I. THE ADSORPTION OF GASES ON PLANE SURFACES OF GLASS, MICA AND PLATINUM. *Journal of the American Chemical Society.* 1918;40:1361-1403.

[40] Pagonabarraga I, Rubí JM. Derivation of the Langmuir adsorption equation from non-equilibrium thermodynamics. *Physica A: Statistical Mechanics and its Applications.* 1992;188:553-567.

[41] Brinkmann RA, King RP. A Kinetic Model Framework for Combined Diffusion and Adsorption Processes. in *Metallurgy*;2(Johannesburg):189-195Southern African Institute of Mining and Metallurgy 1987.

[42] Renneke R, Pasquali M, Hill C. Polyoxometalate systems for the catalytic selective production of nonthermodynamic alkenes from alkanes. Nature of excited-state deactivation processes and control of subsequent thermal processes in polyoxometalate photoredox chemistry. *Journal of the American Chemical Society.* 1990;112.

[43] Ravelli D, Protti S, Fagnoni M. Decatungstate Anion for Photocatalyzed "Window Ledge" Reactions. *Accounts of Chemical Research.* 2016;49:2232-2242.

[44] Pope MT, Müller A. Polyoxometalate Chemistry: An Old Field with New Dimensions in Several Disciplines. *Angewandte Chemie International Edition in English.* 1991;30:34-48.

[45] Goddard JB, Gonas AM. Kinetics of the dissociation of decavanadate ion in basic solutions. *Inorganic Chemistry.* 1973;12:574-579.

[46] Johansson G, Lundgren G, Sillén LG, Söderquist R. On the Crystal Structure of a Basic Aluminium Sulfate and the Corresponding Selenate. *Acta Chemica Scandinavica.* 1960;14:769-771.

[47] Wang M, Muhammed M. Novel synthesis of Al13-cluster based alumina materials. *Nanostructured Materials.* 1999;11:1219-1229.

[48] Johnson GK, Murmann RK, Deavin R, Griffith WP. Sodium and Ammonium Decavanadates(V). in *Inorganic Syntheses*:140-145John Wiley & Sons, Ltd 2007.

[49] Stauffer SR, Peppast NA. Poly(vinyl alcohol) hydrogels prepared by freezing-thawing cyclic processing. *Polymer.* 1992;33:3932-3936.

[50] L. Holloway J, M. Lowman A, R. Palmese G. The role of crystallization and phase separation in the formation of physically cross-linked PVA hydrogels. *Soft Matter.* 2013;9:826-833.

[51] Siepmann J, Siepmann F. Modelng of diffusion controlled drug delivery. *Journal of Controlled Release.* 2012:351-362.

[52] Geisberger G, Paulus S, Carraro M, Bonchio M, Patzke GR. Synthesis, Characterisation and Cytotoxicity of Polyoxometalate/Carboxymethyl Chitosan Nanocomposites. *Chemistry – A European Journal.* 2011;17:4619-4625.

APPENDIX A

A Derivation of the Diaphragm Cell Equation

Fick's First Law is given by

$$J = -\mathscr{D}\frac{\partial C}{\partial x} \tag{A.1}$$

which can be alternatively written

$$\mathscr{D} = -\frac{J}{\frac{\partial C}{\partial x}} \tag{A.2}$$

The flux of material coming into a chamber of fixed volume V through a single surface of cross-sectional area A_c is by definition

$$J = \frac{\partial C}{\partial t}\frac{V}{A_c} \tag{A.3}$$

Substituting A.3 into A.2,

$$\mathscr{D} = -\frac{V}{A_c\frac{\partial C}{\partial x}}\frac{\partial C}{\partial t} \tag{A.4}$$

Now, taking membrane of length L, we can say that over the entire length the quantity $\partial C/\partial x$ is

$$\frac{\partial C}{\partial x} = \frac{C_L - C_0}{L} \tag{A.5}$$

But one of the fundamental assumptions of a diaphragm cell is that the concentration of the sink C_L is zero, giving

$$\frac{\partial C}{\partial x} = -\frac{C_0}{L} \tag{A.6}$$

Substituting A.6 into A.4, we get the final result

$$\mathscr{D} = \frac{VL}{A_c C_0}\frac{\partial C}{\partial t} \tag{A.7}$$

APPENDIX B

Adsorption and Diffusion Solver Program Code

FREUNDLICHPARAMETERSIM.M

```
%FREUNDLICHPARAMETERSIM
% Uses the Crank–Nicholson method to solve for simultaneous Fickian
% diffusion and Freundlich adsorption

% Prepare the workspace for computation
clear
clc
close all

% Declare the physical constants
% Diffusivity of protons in PVA (cm^2 / s)
D = 1.4e-5;
% Diffusivity of protons in water (cm^2 / s)
D_water = 7.0e-5;
% Freundlich preexponential constant
k = [1e-2 1e-3 1e-4];
% Freundlich exponent
n = [0.01 0.1 1];
% Membrane area (cm^2)
A = 7.071;
% Sink volume (cm^3)
V = 223;
% Initial concentration (mol / cm^3)
% Calculated based on pH 2, giving (mol / L), then conversion
C0 = 10^-2;
C0 = C0*1e-3;
% Set time span to 5 min (spectrophotometer interval) (s)
deltat = 5*60;
% Set maximum time to 72 hr (max diffusion cell length) (s)
tmax = 72*60*60;
% Time mesh (s)
t = 0:deltat:tmax;
% Membrane width (cm)
xmax = 0.65;
% Spatial mesh with 10 points (cm)
x = linspace(0, xmax, 10);
% Calculate mesh size
deltax = x(2) - x(1);
% Initial condition (C = C0 @ x = 0, C = 0 everywhere else)
IC = ones(size(x))*10e-9;
IC(1) = C0;
% Boundary condition (C = C0 @ x = 0 for all t)
BC1 = ones(size(t))*C0;

% Declare results matrix
C = zeros(length(x), length(t));

% Add initial and boundary conditions
C(:,1) = IC;
C(1,:) = BC1;

for K = 1:3
    for N = 1:3
        for j = 1:(length(t)-1)
```

```
            % Get the previous time step for simplicity
            Cprevious = C(:,j);

            % Find the values of concentration-dependent diffusivity
            De = freundlichdiffusivity(Cprevious, D, k(K), n(N));

            % Create the coefficients that can be used in matrix form
            beta = De * (deltat/(deltax^2));
            lambda = 2*(1 + beta);
            eps = 2*(1 - beta);

            % Declare the coefficient matrix for the left hand side
            Ccoeff = diag(lambda) + ...
                diag(-beta(1:end-1), -1) + ...
                diag(-beta(2:end), 1);

            % Declare the coefficient matrix for the right hand side
            RCoeff = diag(eps) + ...
                diag(beta(1:end-1), -1) + ...
                diag(beta(2:end), 1);

            % Solve for the values of the RHS
            Cconst = RCoeff*Cprevious;

            % Reinforce boundary conditions
            % https://www.sfu.ca/~rjones/bus864/notes/notes2.pdf
            % Reinforce Left Boundary
            Ccoeff(1,1) = 1;
            Ccoeff(1,2:end) = 0;
            Cconst(1) = C0;

            % Reinforce Right Boundary
            Ccoeff(end,end) = 1;
            Ccoeff(end,1:end-1) = 0;
            Cconst(end) = C(end,j);

            Csols = Ccoeff \ Cconst;

            % For debugging purposes
            % plot(x, Cprevious, x, Csols)

            % Update the profile matrix
            C(:,j+1) = Csols;

            % Do a mass balance for the next right boundary condition
            C(end,j+1) = ((beta(end)*deltax*A)* ...
                (Cprevious(end-1)-Cprevious(end))/V)+C(end,j);
        end

        % Choose the right subplot
        switch K
            case 1
                switch N
                    case 1
                        plotnum = 1;
                    case 2
                        plotnum = 4;
                    case 3
                        plotnum = 7;
                end
            case 2
                switch N
                    case 1
                        plotnum = 2;
                    case 2
                        plotnum = 5;
                    case 3
```

```
                        plotnum = 8;
                end
            case 3
                switch N
                    case 1
                        plotnum = 3;
                    case 2
                        plotnum = 6;
                    case 3
                        plotnum = 9;
                end
        end
        subplot(3,3,plotnum)

        % Plot sink concentration with increasing time
        plot(t,C(end,:));

        % Give labels
        if K == 1
            ylabel(['n = ' num2str(n(N))])
        end
        if N ==3
            xlabel(['K = ' num2str(k(K))])
        end

    end
end
```

FREUNDLICHDIFFUSIVITY.M

```
function De = freundlichdiffusivity(C, D, k, n)
%FREUNDLICHDIFFUSIVITY: Effective concentration-dependent diffusivity based
%on the Freundlich isotherm
%   DE = FREUNDLICHDIFFUSIVITY(C, D, k, n) calculates the effective
%   diffusivity at all concentrations in the vector C where
%     D is a scalar containing the concentration-independent diffusivity
%     k is a scalar containing the Freundlich preexponential constant
%     n is a scalar containing the Freundlich exponent

% Return the values
De = D ./ (k .* n .* (C.^(n-1)) + 1);
```